Metal partitioning and speciation in a mining-impacted estuary by traditional and passive sampling methods

Carlos Ruiz Cánovas[1]*, Maria Dolores Basallote[1], Pedro Borrego[1], Ricardo Millán-Becerro[1], Rafael Pérez-López[1]

* Corresponding autor: carlos.ruiz@dgeo.uhu.es

1. Department of Earth Sciences and Research Center on Natural Resources, Health and the Environment, University of Huelva, Campus 'El Carmen', Fuerzas Armadas s/n, 21071 Huelva, Spain.

Abstract

This study deals with the metal partitioning and bioavailability of metal/loids in the estuary Ria of Huelva (SW Spain) which is strongly affected by historical mining and industrial activities. To address this issue, traditional (i.e., grab samples) and passive sampling (i.e., diffusive gradient in thin films, DGTs) was carried out in the outer part of the estuary during different tidal cycles in order to determine the dissolved and particulate metal/loid concentrations. The dissolved concentrations exceeded, by several orders of magnitude, those reported in other estuaries worldwide that are affected by anthropogenic activities. A spatial pattern was observed in the metal distribution; a decrease seaward was recorded for some of the elements associated with mining (e.g., Cu, Zn, and Cd), the opposite tendency is observed for others associated with harbor emissions (e.g., Sn, Ni, or Pb). A different metal/loid partitioning pattern was also observed; Fe, and to a lesser extent Pb and Sn, were chiefly found in the particulate matter, while the rest of the elements were mainly found in the dissolved form. The bioavailability of the metal/loids

was studied by speciation using both geochemical modeling and DGTs; while concentrations in DGTs supported metal/loid speciation for Zn, Cd, Mn, Co, As, and Sb according to their affinity to form strong or weak complexes, some discrepancies were observed for other elements such as Cu, V, Fe, and Pb, which are prone to forming strong complexes. The main reason behind the unexpectedly high Fe and Pb DGTs concentrations may be associated with their presence in the colloidal particles passing through the DGT. There was a strong positive correlation between dissolved and DGT concentrations for Cd and Mn, and to a lesser extent for Fe and Cu, highlighting the direct relationship between the concentrations in water and availability to living organisms in the estuary.

Keywords: bioavailability; diffusive gradient in thin films (DGT); metal toxicity; metal pollution; passive samplers

1. Introduction

Estuaries are semi-enclosed coastal bodies of water freely connected to the open sea, where the seawater is measurably diluted with freshwater from land drainage (Dyer, 1997). Estuaries are also the key interface between catchments and seawater as the rivers collect and transport accumulated inputs, both natural and anthropogenic, from the whole catchment (Hartnett et al., 2011). Due to the increasing impact of anthropogenic activities, estuaries are considered to be very threatened areas. For example, estuaries have been traditionally used for the disposal of wastes worldwide (Spencer et al., 2006), which have contributed notably to their deterioration. The influence of freshwater inputs, increasing urbanization in estuarine areas, and the related discharges of domestic effluents aggravate the impact of such anthropogenic activities. Consequently, metal pollution is a global

environmental quandary in estuaries as metals are increasingly present in aquatic systems due to the legacy of historical pollution with cumulative effects of anthropogenic metal emissions (Machado et al., 2016).

These increasing metal emissions may pose a great risk for living organisms in estuaries; owing to the high biological productivity in these systems, fisheries flourish in estuaries, acting as a nursery, feeding source, and safehouse for numerous species at different stages of their life cycles (Dantas et al., 2013). For this reason, international policies are required to protect these environmental areas from potential anthropogenic activities. The Water Framework Directive (WFD) (EU Commission, 2000) established a framework for the protection of all surface (rivers, lakes, transitional and coastal waters) and groundwater at European Union (EU) level and aimed to achieve a good ecological and chemical status by 2015. According to the WFD the deterioration of estuaries should be prevented, and their aquatic ecosystem status protected and enhanced. To address this issue, the WFD requires, among other measures, the execution of monitoring programs to evaluate the chemical status of estuarine waters. However, these programs commonly only consider the dissolved fraction of priority substances despite the recommendation of some works about including the need to measure bioavailable forms rather than total or filterable concentrations in the water quality guidelines (e.g., Sherwood et al., 2009; Montero et al., 2012; Montero et al., 2013). This recommendation is based on the fact that metal toxicity and mobility depend not only on the concentration but also on its speciation (Allen, 1993; Guéguen et al., 2011). Therefore, the determination of the labile species of trace metals, in addition to their dissolved and particulate metal concentrations, is of great importance to improve our understanding of the chemical processes that govern their fate, mobility, and impact on aquatic environments, especially in estuaries (Mangal et al., 2016).

Another shortcoming of the traditional spot samplings performed during monitoring programs is the lack of sample representativeness because spot sampling only provides a picture of the conditions at the sampling time (Allan et al., 2007). This is especially relevant in estuaries, which are dynamic and complex systems where their physicochemical characteristics can deeply fluctuate with both tidal and river contributions (Hamilton et al., 2006). This issue has been addressed in other aquatic environments with the installation of autosamplers, which can perform high-resolution samplings to capture sudden hydrochemical changes (e.g., Cánovas et al., 2010; Chapin, 2015). Previous works have studied the use of passive samplers, like diffusive gradient in thin films (DGT), to overcome these limitations (e.g., Dunn et al., 2003, 2007; Montero et al., 2012; 2013; Mangal et al., 2016). The use of DGT offers a reliable and sensitive measurement of DGT-labile metal species, such as the free ionic metal, inorganic complexes, and a fraction of organic complexes (Tusseau-Vuillemin et al., 2004; Guéguen et al., 2011). Conceptually, the DGT provides a time-integrated quantification of labile species in the water that flow through the device during the deployment (Unsworth et al., 2006), thus obtaining the accumulation of the most labile fraction of metals over the whole exposure time, instead of an unrepresentative single measurement (Schintu et al., 2008). However, these devices should be tested in different environments and conditions, especially in aquatic environments strongly affected by metal pollution. An outstanding example of the legacy of metal pollution is the Huelva estuary (SW Spain), which has been intensively affected by mining activities since ancient times and has suffered from pollutant pressure by industry since 1966. Therefore, the main goals of this work are: i) to study the metal partitioning and speciation along a mining-impacted estuary; ii) to determine the metal bioavailability using DGT; and iii) to evaluate the reliability of DGT devices to detect hydrochemical changes associated with tides.

2. Site description

The Huelva estuary, also known as the Ria of Huelva (Fig. 1), is formed by the common mouth of the Odiel and Tinto rivers (SW Spain). Both rivers are deeply polluted by mining activities that have been developed in their drainage basin since ancient times (e.g., Cánovas et al., 2007). This fact makes the Huelva estuary a unique case in the world, as the Tinto and Odiel rivers carry great loads of acidity (pH around 2.5 and 3.5, respectively) and dissolved metals to the estuary: 7900 t yr^{-1} of Fe, 5800 t yr^{-1} of Al, 3500 t yr^{-1} of Zn, 1700 t yr^{-1} of Cu, as well as smaller quantities of other metals and metalloids (Nieto et al., 2007). As a consequence of changes in pH and salinity, some of these metals and metalloids tend to sink into the estuarine sediments, however, the most mobile metals cross the estuary giving rise to a metal-rich plume in the coastal waters of the Gulf of Cádiz (e.g., Van Geen et al., 1991; Elbaz-Poulichet et al., 2001). The hydrochemical properties of the Huelva estuary are strongly controlled by the mixing processes between the volume of acidic river waters and seawater, thus, a progressive increase in pH values and a decrease in the metal concentration is observed along the estuary (e.g., Elbaz-Poulichet et al., 2001). In addition, an increase in the suspended matter is observed, which is physically deposited and redistributed along the estuary by tides coinciding with low energy events (Carro et al., 2018). According to these mixing processes, three different zones can be observed (Carro et al., 2018): i) zone 1, where pH values range between 2.4 and 4.5, the chlorinity is below 3 g L^{-1}, and a large proportion of metals contained in acidic river waters are transferred to the particulate matter (mainly as Fe minerals); ii) zone 2, characterized by pH and chlorinity values ranging from 4.5 to 7.5, and 3 to 15 g L^{-1}, where the metal removal (as Al minerals) is also intense; and iii) zone 3, characterized by slightly basic pH values (7.5–8.2), where the salt-induced mixing

process that is typical of estuarine systems occurs and the occurrence of dissolved metal/loids is limited to only those following a quasi-conservative behavior (e.g., Zn and Cd) and others suffering re-dissolution and/or desorption from the particulate phase (e.g., U, Cu and As). These three zones move along the estuary over the hydrological year due to changes in the proportion of river and seawater; thus, during periods of low fluvial inputs, the tidal influence area moves upstream causing the mixing zone to be pushed northwards. Changes in the water contribution also lead to different mixing models in the estuary, which is partially stratified during the rainy season, and homogeneously mixed during the dry season, when the river flow is less than 6 $m^3 s^{-1}$ (Carro et al., 2018).

3. Methodology

3.1. Sampling

Water samples were collected periodically (0, 6, 24, and 30 h) during a 30 h period (25–26 July 2018) at four sampling stations (T1–T4) (Fig. 1), to include two tidal cycles (two low and high tide cycles). The sampling took place in the summer when the Tinto and Odiel rivers show the lowest flows through the year (Cánovas et al., 2007). Due to the low fluvial inputs (less than 6 $m^3 s^{-1}$) recorded during the sampling, all the stations would belong to the zone 3 previously described by Carro et al., (2018), reflecting the conditions of homogeneous water mixing, consequently, samples were collected a few centimeters below the surface. The tidal range during the sampling was around 1 m, reflecting micro-tidal conditions. The sampling was not intended to comprise the whole estuary but zones that are highly influenced by seawater; sampling points were selected within zone 3 due to the abundance of living organisms and to the different influences of anthropogenic activities. T1 is in the Tinto estuary and receives both the mining influence of the Tinto river and the industrial impact by leakages from the phosphogypsum stack (Fig. 1), which

150 releases significant loads of metal/loids into the estuary (Pérez-López et al., 2016). T2
151 and T3 are in the outer part of the Odiel estuary and are affected by mining inputs from
152 the Odiel river, although the latter point (T3) may also be influenced by the Tinto river
153 discharges during high tides (Fig. 1) and by recreational boat activities. Finally, T4 is the
154 outer sampling point within the Ria of Huelva estuary, where the influence of seawater is
155 larger and it is close to a harbor where recreational ships tie up (Fig. 1). The sediments
156 from this latter point tend to show toxicity due to Cu, As, Pb, and Zn, as previously
157 reported by Basallote et al. (2018).

158 Filtered samples (0.45 μm pore size Millipore filters) were collected in high-density
159 polyethylene (HDPE) bottles, acidified to pH < 2 with nitric acid 65% Merck Suprapur®,
160 and stored in a refrigerator until analysis. Raw samples (not filtered but acidified) were
161 also collected to study metal particulate transport along the estuary. Thus, the difference
162 between the concentrations in the filtered and unfiltered samples will be associated with
163 the particulate matter. In addition, filtered but non-acidified samples were also collected
164 for anion (i.e., Cl^-, Br^-, F^-, NO_3^-, PO_4^{3-}) determinations. All the bottles that were used
165 during the sampling were acid-washed (10% HCl) for 24 h, rinsed in Milli-Q water (18.2
166 MΩ, Millipore) and stored in sterile plastic bags prior to use.
167

168 **3.2. DGT devices settlement**

169 In order to study metal bioavailability in estuarine waters, DGT devices were placed in
170 sampling stations in duplicate. In these devices, free cations and labile metal complexes
171 (labile fraction) are diffused through a cellulose nitrate filter (0.45 μm porosity) and a
172 diffusive gel as a result of a concentration gradient, and then they accumulate in a
173 chelating resin gel Chelex-100. In summary, the DGT passive samplers tend to collect
174 the labile fraction of metals that show affinity to the chelex-100 resin. The LSNX-NP

175 Loaded DGT device (DGT® Research) used in this study is a standard DGT holder for
176 solutions with 0.8 mm APA diffusive gel, a polyethersulphone filter membrane, and a
177 mixed binding layer of Chelex and titanium oxide (Metsorb). This device is especially
178 designed to measure up to 40 metals (Panther et al., 2014). After about 12 and 24 h of
179 exposure, the DGT devices were retrieved, rinsed with distilled water, and transported to
180 the lab in sterile plastic bags, where a specific determination protocol was followed
181 (Ardelan et al., 2009; Basallote et al., 2020). The DGT devices were dismantled and each
182 of the resin gels (Chelex 100-gel) were placed in separated acid washed polyethylene
183 vials with 1 mL ultrapure HNO_3 (3 M), followed by agitation at 60 rpm for 24 h. The
184 elution extracts were diluted with Milli-Q water to 5 mL, prior to metal determination.
185
186 DGT concentrations were determined using Eq. (1):
187 $$C_{DGT} = \frac{MDGT\Delta g}{DtA}, \qquad \text{Eq. (1)}$$
188 where C_{DGT} is the concentration of metal in the bulk solution measured by the DGT unit,
189 M_{DGT} is the mass of the analyte accumulated on the binding layer, Δg is the thickness of
190 the diffusive gel (0.078 cm) plus the thickness of the filter membrane used (0.014 cm), D
191 is the diffusion coefficient of each metal ($cm^2\ s^{-1}$) (see Supplementary Data, Table SM1),
192 t is deployment time (s, exact time for each exposure period), and A is the DGT cross-
193 sectional exposure area (3.14 cm^2).

194 **3.3. Analytical determinations and data treatment**

195 Temperature, pH, electrical conductivity (EC), and oxidation-reduction potential (ORP)
196 were measured in situ using HANNA HI 98190 and 98192 portable meters. A three-point
197 calibration was performed for both EC (147 µS/cm, 1,413 µS/ cm, and 12.88 mS/cm) and
198 pH (4.01, 7.00, and 9.21), while the ORP was controlled using two points (240 and 470

mV). The salinity (S) was calculated from Cl^- concentrations, according to the following equation: $S = 1.805\ Cl^-\ (g\ L^{-1}) + 0.03$ (Chester, 1990). Trace metal/loid determination in the water samples and the DGT elution extracts were performed by iCAP TQ ICP-MS at the HydroSciences laboratory of the University of Montpellier. Estuarine water reference material for trace metals (SLEW-3) was also analyzed to check the analytical accuracy. In addition, the anions (i.e., Cl^-, Br^-, F^-, NO_3^- and NO_2^-) were determined using ion chromatography (Dionex DX-120) at the R+D laboratories of the University of Huelva, and the total alkalinity was determined by CHEMetrics® Total Titrets®, with a range of 10–100 or 100–1000 mg L^{-1} as $CaCO_3$ equivalents.

Information about the speciation of elements was obtained by the PHREEQC code v. 3.4 (Parkhurst and Appelo, 2013) using the Truesdell-Jones equations-based LNLL thermodynamic database (Johnson et al., 1992), which provides accurate activity calculations in chloride dominated solutions with ionic strengths below 1 mol/L, and it is more complete than other databases. The ORP measurements were corrected to the standard hydrogen electrode to calculate Eh (Nordstrom and Wilde, 1998), which was used to input pE values for the geochemical modeling. The balance error obtained by the PHREEQC code was below 10% for all the samples. For consistency, the PHREEQC outputs were compared with the chemical speciation obtained using the CHEAQS program version 2017.3 (Verweij, 2017). The CHEAQS model includes inorganic speciation and the mineral equilibrium based on the National Institute of Standards and Technology database version 8.0 (NIST, 2004). Similar speciation results were obtained from both codes.

A Principal Component Analysis (PCA) was performed on the dissolved and DGT concentrations to ascertain the patterns of behavior in the variables and samples. PCA

reduces the number of variables in a multivariate data set, whilst retaining most of the variation that is present in the data set. Variables were z-scores standardized to fit a normal distribution, and therefore the Pearson (n − 1) correlation matrix was used (Davis, 2002).

4. Results and discussion

4.1. Metal/loid partitioning along the estuary

Table 1 shows the main physicochemical properties of the samples collected along the estuary. As can be seen, the chlorinity of the samples ranged from 18 to 20 g L^{-1}, with mean pH values of 8.2±0.2. The highest pH and chlorinity values were observed in the outer sampling station of the estuary (T4; 8.2–8.4 and 19–20 g L^{-1}) for both low and high tides, while slight fluctuations in the pH between low and high tides were observed at T1 and T2. Figure 2 illustrates the evolution of the dissolved metal/loid concentrations (triangle dashed line) along the estuary. As expected, the metal concentrations in the inner part of the studied sector (T1 and T2) tend to be much higher than in the outer part (T3 and T4) because the influence of pollutant river inputs is higher upstream and diluted seaward by the flushing of cleaner marine water inside the estuary. As a consequence, the metal/loid concentrations at the sampling points were low when compared with the river and upper sections of the estuary (e.g., Hierro et al., 2014a; Olías et al., 2019); i.e., dissolved elements ranged from 194 to 10 μg L^{-1} of Mn, 121 to 14 μg L^{-1} of Zn, 100 to 2.4 μg L^{-1} of Fe, 43 to 6.9 μg L^{-1} of Cu, 16 to 2.6 μg L^{-1} of As, 15 to 0.30 μg L^{-1} of Pb, 5.6 to 0.19 μg L^{-1} of Co, 3.7 to 0.11 μg L^{-1} of Cd, 1.7 to 0.92 μg L^{-1} of V, 2.1 to 0.26 μg L^{-1} of Sb, 0.47 to 0.01 μg L^{-1} of Ni, and 0.16 to 0.01 μg L^{-1} of Sn for the different tidal periods (Fig. 2). The progressive mixing of alkaline seawater with the acidic waters of the Tinto and Odiel rivers promotes the strong decrease in the concentration of most

248 metals transported by these acidic rivers. However, some elements deviate from this
249 tendency. For instance, although dissolved Fe concentrations peaked at T2 (100 μg L^{-1};
250 Fig. 2), slightly higher concentrations were observed in the outer sampling stations (T3
251 and T4) than in the inner ones (T1 and T2). More evident is the case for Ni, Pb, and Sn,
252 which had higher dissolved concentrations in T3 and T4 than in T2, and in some cases,
253 than in T1 (Fig. 2). The increasing concentrations for these elements could probably be
254 explained by the intense boating activities in this area, where a recreational harbor is
255 located (Fig. 1). It has been widely reported that these elements in antifouling paints and
256 fuels can be leached into estuarine waters and sediments (e.g., Turner, 2014; Ytreberg et
257 al., 2016). This behavior of the elements is also suggested by the PCA carried out on the
258 samples (Fig. SM1a). The first component (F1) explains 46% of variance and seems to
259 be related to the fluvial influence of the samples; the higher the riverine influence, the
260 higher the positive values of F1. On the other hand, the second component (F2) seems to
261 be related to the origin of the variables; thus, most of the metals associated with mining
262 (i.e. Cu, Cd, Mn, As, Co, and Sb) are located on the negative side of F2, while those
263 elements associated with seawater or fuel/antifouling (i.e., Cl, Br, Pb, Sn) are on the
264 positive side. Another striking fact is the existence of tide-driven variations in some metal
265 concentrations. As can be seen in Figure 2, some dissolved elements such as Cd, Zn, Mn,
266 and to a lesser extent Cu, V, or Sb, follow a zig-zag evolution over time according to the
267 tidal regime (low-high), especially in the inner part of the estuary (T1-T2), where the tidal
268 influence is higher. These fluctuations in metal/loid concentrations were also observed
269 by Hierro et al. (2014a), who reported variations in dissolved elements concentrations
270 (i.e., Mn, Zn, Cu, Co, Cd, and Ni) during the tidal cycle in the inner part of the Tinto river
271 estuary.

Concerning particulate matter, high concentrations were mainly recorded for Fe (up to 745 μg L^{-1}), and to a lesser extent for Cu and Zn (up to 19 μg L^{-1}), Mn (14 μg L^{-1}), and Pb (12 μg L^{-1}). This contrasts with the low particulate concentrations observed for some other elements (e.g., Cd, Sb, Sn, or V), which in some cases were even below the detection limit (Fig. 2). Therefore, a different metal/loid partitioning pattern can be observed among the studied elements. Figure 3 represents the dissolved fraction contribution for each element as box and whiskers plots. The length of the box represents the interquartile range, which comprises 50% of the values, while the horizontal line inside the box represents the median and the inner square of the mean value. The whiskers are lines that lengthen from the box to the highest and lowest values excluding outliers (*), which represent those values being 1.5 higher than the length of the box from its upper or lower border. As can be clearly seen, there is a group of elements composed of Zn, As, Cd, Ni, and V, which were mostly present in estuarine samples in the dissolved fraction (interquartile range (IR) of 85–100%; Fig. 3). On the other hand, Fe is chiefly present in the particulate matter (IR of dissolved fraction between 2.5 and 3.9%). The higher concentration of Fe in the particulate matter than in the dissolved fraction is consistent with previous works along the estuary that report intense Fe precipitation processes (e.g., Achterberg et al., 2003; Hierro et al., 2014a,b). Other elements that were abundant in the particulate matter were Pb (IR of 37–59% of the dissolved fraction), and to a lesser extent Cu, Mn, Co, Sn, and Sb, that recorded some values of dissolved fraction between 45 and 67% (Fig. 3). Vicente-Martorell et al. (2009) also reported the abundant presence of Pb and Cu in the particulate fraction along the Ria of Huelva estuary. The presence of As, Pb, Zn, Cu, Mn, and Co in the particulate matter during mixing processes has been also previously reported and was estimated to be around 60–90% of the total concentration (Hierro et al. 2014a). These authors stated that these elements undergo intensive sorption

297 processes onto Fe and Al precipitates along the maximum turbidity zone (zones 1 and 2;
298 Carro et al., 2018), where lower salinity and pH values are observed. However, the
299 increase in the pH and salinity in the outer zone of the estuary, where the samples were
300 collected in our study, may have caused desorption processes and the formation of
301 aqueous complexes, enhancing their presence in the dissolved form. This fact may explain
302 the lower values of particulate matter observed for these elements (especially for As) in
303 our study compared with those reported by Hierro et al. (2014b).

304 **4.2. Metal speciation and bioavailability along the estuary**

305 The concentrations reported in this study are considerably higher than those observed in
306 other estuaries around the world that are deeply affected by anthropogenic activities (e.g.,
307 Benoit et al., 2010; Gaonkar and Matta, 2019; Hatje et al., 2003; Thanh-Nho et al., 2018),
308 even at higher salinities (Table 2) than those reported in these studies. However, metal
309 toxicity and mobility depend not only on the concentration but also on the speciation
310 (Allen, 1993; Guéguen et al., 2011; Millero et al., 2009); thus, those metals forming
311 strong complexes with ligands may not be available to organisms, and only the labile
312 fraction of the metal concentration would be available to them (Amato et al., 2014).
313 Therefore, a different complexation pattern was inferred among the divalent metals
314 studied (i.e., Cu, Zn, Mn, Cd, Co, Pb and Ni). For example, Ni, Mn, and Co were mainly
315 found as free species (Free-Me; average of 85, 60, and 58% of Ni^{2+}, Mn^{2+}, and Co^{2+}
316 respectively; Fig. 4A), with minor quantities of sulfate (32, 18, and 14% of $CoSO_{4(aq)}$,
317 $MnSO_{4(aq)}$, and $NiSO_{4(aq)}$, respectively) and chloride complexes (20, 4.8, and 1.4% of
318 $MnCl^{+}$, $CoCl^{+}$, and $NiCl^{+}$, respectively; Fig. 4A). On the other hand, Cd and to a lesser
319 extent Pb are mainly forming Cl complexes (99 and 66%, respectively; i.e., $MeCl^{+}$,
320 $MeCl_2$, and $MeCl_3^{-}$). Zinc shows a more balanced speciation between free and chloride
321 species (39% of Zn^{2+} and 47% of Cl complexes; Fig. 4A). However, Cu speciation is

322 mainly dominated by Cu carbonate species ($CuCO_{3(aq)}$), with 62% of the total species in
323 this form, followed by hydroxyl (i.e., 20% of $CuOH^{+}$), free (7.6% of Cu^{2+}), and around
324 5% of chloride complexes and 5% of sulfate complexes (Fig. 4A). Fe, Sb, and Sn (Fig.
325 4A and Table SM2) are chiefly found as hydroxyl complexes, where the uncharged
326 hydroxyl complexes are predominant (i.e., 99% of $Sn(OH)_{4(aq)}$ and $Sb(OH)_{3(aq)}$, and 92%
327 of $Fe(OH)_{3(aq)}$). On the other hand, As and V(Table SM2) are primarily found as arsenate
328 (AsO_4^{3-}) and vanadate species, respectively (90–100% of total species; Table SM2).
329 Considering the charge of the species (Fig. 4B and Table SM2), a different trend is
330 observed among the elements; Ni (84%), Mn (79%), and Zn (51%) are mainly found to
331 form positively charged species, while Fe, Sn, Sb (all of them around 99% of the total
332 species), and Cu (64%) are mostly found as uncharged species (Fig. 4B). Metals like Cd
333 and Pb, show a balanced speciation between the uncharged and positively charged species
334 (Fig. 4B). In contrast, As and V are chiefly found as negatively charged species (around
335 100%).

336 As shown in Table 3, the concentrations retained by the DGTs (C_{DGT}) in the Ria of Huelva
337 are high for some of the elements studied: between 33 and 165 μg L^{-1} of Zn, 4.8 and 61
338 μg L^{-1} of Mn, 8.1 and 45 μg L^{-1} of Fe, 4.6 and 23 μg L^{-1} of Cu, 0.30 and 8.0 μg L^{-1} of Pb,
339 0.07 and 8.7 μg L^{-1} of Co, and lesser amounts of Cd (0.10–2.3 μg L^{-1}), V (0.85–1.3 μg L^{-1}),
340 As (0.12–1.3 μg L^{-1}), Sn (0.04–0.41 μg L^{-1}), and Sb (0.02–0.21 μg L^{-1}). Comparing the
341 C_{DGT} observed in this study with those reported in other estuarine systems, the C_{DGT} are
342 generally higher than those observed in Runaway Bay Marina (Australia), an estuarine
343 system strongly affected by harbor activities and the input of storm water from the
344 surrounding urban area (Shiva et al., 2016). Only for those metal/loids forming oxyanions
345 (i.e., As, V, and Sb), were the C_{DGT} values in Runaway Bay similar or slightly higher than
346 in the Ria of Huelva. Most of values in this study were also higher than those reported in

other studies of estuaries in Spain, Brazil, and China, that are affected by human activities (Table 3). Only some of the values from other studies exceeded those reported in the Ria of Huelva estuary; for example, a C_{DGT} of up to 195 μg L^{-1} for Zn and 26 μg L^{-1} for Ni, (Table 3) were found in the Jiulong estuary (China) which is characterized by strong metal contamination due to industrial activities.

The labile fraction is operationally defined as the labile forms of metals including free metal and weak metal–ligand complexes (Millero et al., 2009). Generally, the lability of metals is strongly controlled by their charges; metals with higher charges may bind more tightly to the ligands. Another factor that controls the strength of the ionic bonds is the size of the ion; thus, ions with smaller atomic radii form stronger bonds than ions with larger radii. Considering the dominant species in the estuarine waters (Fig. 4A), those metals that are mostly found as free or weak metal complexes (e.g., Free-Me, Cl- Free-Me species) such as Cd, Co, Mn, Ni, Pb, or Zn may be more labile than others, such as Cu, Fe, Sn, As, V, or Sb, which are mainly found as carbonate or hydroxyl complexes. The labile trace metals in marine environments generally make up a small percentage of the total dissolved concentrations, such as the free metal ions and the most labile trace metal complexes (Gao et al., 2019). Thus, it is important to determine these essential trace elements within the dissolved phase, as this small and labile fraction is expected to be the most bioavailable fraction for living organisms (Baeyens et al., 2011). This is in agreement with the C_{DGT} values (DGT_{Labile}, Fig. 5) observed for elements such as Zn, Cd, and Co which account for a high percentage of the 0.45 μm filtered dissolved concentration (Fig. 5), or even in some cases (Zn and to a lesser extent Co) exceed the dissolved concentration. On the other hand, the C_{DGT} values for As and Sb were low considering their affinity for forming strong complexes (0.1–3.0% and 1.3–5.5% of the dissolved concentration, respectively; not shown in Fig. 5). However, some discrepancies

for other elements were observed regarding their affinity to form labile complexes. For example, Cu and Mn showed a similar lability, with C_{DGT} values of 36–59% and 30–38% of the dissolved concentration, respectively (Fig. 5), despite the higher affinity of Cu to form strong complexes compared with the higher lability of Mn. In this sense, V also exhibited a higher lability than expected, with a C_{DGT} around 25–49% of dissolved concentrations (not shown in Fig. 5). However, the most outstanding result was the extremely high C_{DGT} values observed for Fe, Sn, and Pb at 12 h, with the maximum C_{DGT} exceeding between two and five times the average dissolved concentration observed in the water column (Fig. 5). This fact may be related to the ability of colloids to be captured in the DGT devices (Gao et al., 2019), since both metals were ubiquitously found in the particulate matter in the estuarine samples (Fig. 2). The behavior of these elements (i.e. Fe, Sn, and Pb) can be clearly seen in the PCA performed on the DGT concentrations (Fig. SM1b). The first component explains 50% of variance and may be related to the affinity of elements in the dissolved or particulate phases; thus, elements related to the particulate phase are located on the negative side whereas those related to the dissolved phase are on the positive side. As can be seen, the sampling points with a higher seawater influence (i.e., T3 and T4) are on the negative side. The second component explains 21% of variance and seems to be related to the time of deployment of the DGT devices; all of the DGT devices that were exposed for over 12 h are located on the positive side while those that were exposed for over 24 h are placed on the negative side.

Vicente-Martorell et al. (2009) studied the bioavailability of metals along the same estuary, based on their lability. Although these authors did not cover all the metal/loids studied in this work, they proposed the following metal availability ranking order: Cd > Zn > Cu > Pb. This order differs from that obtained in this study (Zn > Cu > Pb > Cd),

397 which is probably due to the transference of metals from the particulate matter to the DGT
398 device for some elements, especially Pb and Zn. Considering the correspondence between
399 the metal/loid absorption by the DGT and the biological membranes in organisms
400 (Baeyens et al., 2011; Zhang and Davison 2000), the accumulation of some metal/loids
401 in the DGTs correlates with the labile metal fraction potentially accumulated by estuarine
402 living organisms. Furthermore, as has been previously mentioned, the labile trace metals
403 in the marine environment comprise only a percentage of the total dissolved metal
404 concentrations. Morillo and Usero (2008) reported high concentrations of Zn, Cu, Mn,
405 Cd, and As in barnacles (B. *Amphitrite*) collected along the Ria of Huelva estuary, which
406 seemed to be strongly correlated with their dissolved concentrations. Also, Vicente-
407 Martorell et al. (2009) reported positive correlations between metals in fish tissues and
408 water concentrations, especially for gilt-head bream (*S. aurata*), a pelagic fish commonly
409 found in the water column. Based on these correlations, the ability of DGTs to mimic
410 metal/loid bioavailability to living organisms in the Ria of Huelva estuary could be
411 evaluated by comparing the concentrations in both the water (filtered and non-filtered
412 samples) and the DGTs. Figure 6 shows the relationship between the dissolved metal
413 concentrations and DGTs in the estuary. For Cd and Mn, there is a strong positive
414 correlation between the dissolved and DGT concentrations (R^2 = 0.91–0.94). Although
415 with poorer correlation coefficients, the same tendency of increasing DGT values with
416 dissolved concentrations was observed for Fe (R^2 = 0.59) and Cu (R^2 = 0.58), and to a
417 lesser extent Sb (R^2 = 0.40), and Co (R^2 = 0. 37). However, positive correlations for Fe
418 and Sb may be due to only one extreme value (Fig. 6). Weaker or no correlations were
419 observed for Pb (R^2 = 0.13), Sn (R^2 = 0.05), Zn (R^2 = 0.03), and V (R^2 = 0.02) (the latter
420 not represented). These values disagree with those previously found by Dunn et al. (2003)
421 between the 24 h DGT-labile and dissolved (0.45-µm filtered samples) concentrations

422 reported in Gold Coast Broadwater (Australia) for Cu ($R^2 = 0.96$), Pb ($R^2 = 0.68$), and Zn
423 ($R^2 = 0.91$). Except for Zn, this study also points out the direct relationship of metal/loid
424 concentrations and metal exposure previously reported by Morillo and Usero (2008) in
425 estuarine living organisms. On the other hand, the correlations observed between
426 particulate and DGT concentrations for those elements that are prone to being present in
427 the particulate matter, i.e., Fe, Pb, Sn, or Cu, were low or inexistent ($R^2 = 0.18$ for Sn,
428 $R^2 = 0.17$ for Pb, $R^2 = 0.08$ for Cu, and $R^2 = 0.02$ for Fe).

429 **4.3. Validation of DGT devices as monitoring tools for metal/loid exposure**

430 Water quality monitoring programs frequently require a high number of samples for
431 analysis, although this conventional approach only captures short events, especially in
432 complex systems like estuaries. The use of DGT devices as a monitoring tool for labile
433 trace metal concentrations in dynamic estuarine and coastal waters has been successfully
434 tested, avoiding the risk of sample contamination, the difficulty of preserving samples,
435 and other issues related to conventional samplings (Gao et al., 2019). Although it is
436 possible to establish a direct relation between metal availability to living organisms (i.e.,
437 by DGT accumulated concentrations) and dissolved metal concentrations (Fig. 6), in most
438 cases the use of DGTs cannot replace the determination of dissolved concentrations since
439 both values can be different by some orders of magnitude. Lucas et al. (2015) reported
440 DGT-measured concentrations of Cu and Co that were considerably lower than filtered
441 water measurements and only the Mn and Zn concentrations were similar to the filtered
442 ones. A comparison of DGT with dissolved concentrations in UK freshwaters determined
443 using cross flow ultrafiltration (nominal size of 1 kDa), by Liu et al. (2013), showed
444 similar concentrations for a number of elements (e.g., Mn, Zn, and Cr) but lower DGT-
445 measured concentrations for other elements (e.g., Al, Cd, Co, Cu, Fe, and Pb). The main
446 reason stated by these authors for these differences is the ability of these latter metals to

447 form kinetically inert species or thermodynamically stable complexes, leading to a lower
448 binding by the DGT resin layer. In this context, Figure 7 shows the relationship between
449 the average content of labile species (Me^{2+}, Cl-Me; from geochemical modelling) for all
450 the metal/loids studied and the percentage of C_{DGT} with respect to the dissolved
451 concentration in the water column (except for Fe, Pb and Sn, which the total concentration
452 (dissolved and particulate) was used instead). As can be seen, there are some metal/loids
453 such as As, Sb, Cd, Co, Mn, Cu, and Zn, which showed a relatively good agreement
454 between both variables, although some of these metals (e.g., Cu and Zn) showed higher
455 C_{DGT} than expected (around 60 and 100% of filterable concentrations), considering the
456 liability of their dissolved species. Dunn et al. (2003) reported DGT-labile measurements,
457 as a fraction of filterable concentrations, of only 21 to 27% for Cu and Zn. Slightly higher
458 values were also obtained by Cindríc et al. (2017) in a small marine harbor of the Adriatic
459 Sea (Croatia) with a C_{DGT} of around 32–54% for Cu, 45–56% for Zn, 52–56% for Co and
460 Cd, and 70–90% for Cd. Despite this fact, this is a good validation of the use of DGT
461 devices as a monitoring tool for most metals. A poor performance was in turn obtained
462 for other metals such as V and Ni (not represented); while the C_{DGT} were higher than those
463 expected for V considering its lability (Fig. 7), Ni was not even detected despite its higher
464 lability. On the other hand, metals such as Fe, Pb, and Sn had C_{DGT} around two to five
465 times higher than the dissolved concentrations in the water column (Fig. 5), despite the
466 low lability of their species (Fig. 7). Higher DGT concentrations in comparison with those
467 measured directly in solution were previously reported by Davison and Zhang (2012) and
468 were attributed to differences in the geometric area and in the diffusive boundary layer
469 (DBL). Another factor leading to higher DGT concentrations than dissolved
470 concentrations is the abundance of colloids, which could transfer some metals from the
471 solids directly to the DGT resin (Gao et al., 2019). Ardelan et al. (2009) also suggested

that some particulate-bound metals (i.e., Al and Cd) associated with the particulate fraction (> 0.2 μm) are able to diffuse and be retained by the DGT chelating resin under certain physicochemical changes. This fact is especially relevant in the Ria of Huelva estuary, where the mixing of acidic metal rich waters with alkaline seawaters induces the intense precipitation of Fe and Al-rich colloids. As can be seen in Figure 7, metals such as Pb and Sn, abundant in the particulate matter, had a C_{DGT} that was higher than total concentrations (dissolved + particulate), while around 20% of the total Fe concentration was retained by the DGT. These results highlight the importance of both traditional grab and passive samplings. Thus, the information provided by both methods (i.e., conventional sampling and use of DGTs) may complement each other during monitoring programs of estuaries and coastal areas.

Conclusions

This study investigates the metal partitioning and availability in an estuary strongly affected by historical mining and industrial activities in SW Spain. The metal/loid concentrations recorded along the estuary were high; up to 194 μg L^{-1} of Mn, 121 μg L^{-1} of Zn, 100 μg L^{-1} of Fe, 43 μg L^{-1} of Cu, and so on; the values were several orders of magnitude higher than those registered in others estuaries worldwide that are affected by anthropogenic activities.

A metal partitioning pattern is observed in the outer part of the estuary; while Fe (96–98% of total) and to a lesser extent Pb (41–63%), Cu, Mn, Co, and Sb (33–55%) were found to be abundant in the particulate matter, the rest of the elements (i.e., Zn, As, Cd, Ni, and V) that were studied were chiefly transported in the dissolved phase. Although other authors previously reported that the content of these metal/loids (i.e., As, Pb, Zn, Cu, Mn and Co) in the particulate matter was around 60–90% of total concentration, the

497 lower values found in this study may be related to the location of the samples at the outer
498 zone of the estuary (at higher pH and salinity values), where re-dissolution and/or
499 desorption processes and the formation of aqueous complexes may enhance their
500 presence in the dissolved form.

501 A different complexation pattern was also observed in the estuarine waters. Ni, Mn, and
502 Co were mainly found as free species, whereas Cd and to a lesser extent Pb were mainly
503 forming Cl complexes. Zinc showed a more balanced speciation between free and
504 chloride species (39% of Zn^{2+} and 47% of Cl-complexes), while Cu speciation was
505 mainly dominated by carbonate species (62% of total species). Fe, Sb, and Sn were
506 primarily found as hydroxyl complexes, where the uncharged hydroxyl complexes were
507 predominant (i.e., 99% of $Sn(OH)_{4(aq)}$ and $Sb(OH)_{3(aq)}$, and 92% of $Fe(OH)_{3(aq)}$). On the
508 other hand, As and V were mainly found as arsenate and vanadate (VO_4^{3-}) species (90–
509 100% of total species), respectively.

510 The concentrations retained by DGTs (C_{DGT}) in the Ria of Huelva were generally higher
511 than C_{DGT} values reported in others estuaries worldwide (e.g., up to 165 μg L^{-1} of Zn,
512 61μg L^{-1} of Mn, 45 μg L^{-1} of Fe, 23 μg L^{-1} of Cu, and 2.3 μg L^{-1} of Cd), and were only
513 surpassed by values for some elements that were recorded in estuaries that are extremely
514 polluted by industrial discharges. The speciation data are in agreement with the C_{DGT}
515 observed for elements such as Zn, Cd, and Co, which commonly form labile species, and
516 C_{DGT} accounted for a high percentage of the dissolved concentration. A similar case was
517 observed for As and Sb, whose C_{DGT} values were low considering their affinity for
518 forming strong complexes. However, some discrepancies were observed for other
519 elements such as Cu, V, Fe, Sn, and Pb, with the latter ones with a maximum C_{DGT} that
520 was more than two to five times higher than the dissolved concentration observed in the

521 water column. These discrepancies may be related to the ability of colloids to be captured
522 in the DGT devices since Fe, Sn, and Pb were ubiquitous in the particulate matter in the
523 estuary, but the reason for Cu and V remains unclear.

524 The strong correlation observed between the C_{DGT} and dissolved concentration for some
525 metals, which was previously correlated with metal bioaccumulation in the same
526 estuarine waters, highlights the direct relationship between metal/loid concentrations and
527 metal exposure. The results obtained in this study will contribute to the DGT databases,
528 which include DGT measurements from water bodies worldwide, especially for complex
529 and dynamics systems such as estuaries. However, this research must be extended to other
530 hydrological conditions, such as river flood conditions, when the influence of the Tinto
531 and Odiel rivers is greater on the estuarine waters, or other tidal range conditions (i.e.
532 meso and macro-tidal) where the oscillations in metal concentrations may be greater.
533

534 **ACKNOWLEDGEMENTS**

535 This work was supported by the Spanish Ministry of Economy and Competitiveness
536 through the research project CAPOTE (CGL2017-86050-R) and by the CEIMAR
537 Excellence Research Campus through the project CEIMAR-CEIJ-005. M.D. Basallote
538 thanks the Spanish Ministry of Science and Innovation for the Postdoctoral Fellowship
539 granted under application reference IJC2018-035056-I. The authors would also like to
540 thank to the Co Editor-in-Chief Dr. Damiá Barceló and two anonymous reviewers for the
541 support and comments that notably improved the quality of the original paper.
542
543

544 **APPENDIX A. Supplementary data**

545 Supplementary data to this article can be found online at hppt:

546 **REFERENCES**

547

548 Achterberg, E.P, Herzl, V.M.C, Braungardt, C.B, Millward, G.E, 2003. Metal behaviour
549 in an estuary polluted by acid mine drainage: the role of particulate matter. Environ Pollut
550 121, 283-292. https://doi.org/10.1016/S0269-7491(02)00216-6.

551

552 Allan, I.J., Knutsson, J., Guigues, N., Mills, G.A., Fouillac, A.M., Greenwood, R., 2007.
553 Evaluation of the Chemcatcher and DGT passive samplers for monitoring metals with
554 highly fluctuating water concentrations. J. Environ. Monit. 9 (7), 672-681.
555 https://doi.org/10.1039/b701616f.

556

557 Allen, H.E., 1993. The significance of trace metal speciation for water, sediment and soil
558 quality criteria and standards. Sci. Total Environ. 134, 23-45.
559 https://doi.org/10.1016/S0048-9697(05)80004-X.

560

561 Amato, E.D., Simpson, S.L., Jarolimek, C.V., Jolley, D.F., 2014. Diffusive gradients in
562 thin films technique provide robust prediction of metal bioavailability and toxicity in
563 estuarine sediments. Environ. Sci. Technol. 48, 4485–4494.
564 https://doi.org/10.1021/es404850f.

565

566 Ardelan, M.V., Steinnes, E., Lierhagen, S., Linde, S.O., 2009. Effects of experimental
567 CO_2 leakage on solubility and transport of seven trace metals in seawater and sediment.
568 Sci. Total Environ. 407, 6255-6266. https://doi.org/10.1016/j.scitotenv.2009.09.004.

569

570 Basallote, M.D., Rodríguez-Romero, A., De Orte, M.R., DelValls, T.A. and Riba, I.,
571 2018. CO2 leakage simulation: effects of the pH decrease on fertilisation and larval
572 development of Paracentrotus lividus and sediment metals toxicity. Chemistry and
573 Ecology, 1-21. https://doi.org/10.1080/02757540.2017.1396319.
574
575 Basallote, M.D., Borrero-Santiago, A.R., Cánovas, C. R., Hammer, K. M., Olsen, A. J.
576 and Ardelan, M.V., 2020. Trace metal mobility in sub-seabed sediments by CO2 seepage
577 under high-pressure conditions. Sci. Total Environ. 700, 134761.
578 https://doi.org/10.1016/j.scitotenv.2019.134761.
579
580 Benoit, M., Kudela, R.M., Flegal, R., 2010. Modeled trace element concentrations and
581 partitioning in the San Francisco estuary, based on suspended solids concentration.
582 Environ. Sci. Technol. 44, 5956–5963. https://doi.org/10.1021/es1001874.
583
584 Cánovas, C.R., Olías, M., Nieto, J.M., Sarmiento, A.M., Cerón, J.C., 2007.
585 Hydrogeochemical characteristics of the Tinto and Odiel Rivers (SW Spain). Factors
586 controlling metal contents. Sci. Total Environ., 373, 363–382.
587 https://doi.org/10.1016/j.scitotenv.2006.11.022.
588
589 Cánovas, C.R., Olías, M., Nieto, J.M., Galván, L., 2010. Wash-out processes of evaporitic
590 sulfate salts in the Tinto river: hydrogeochemical evolution and environmental impact.
591 Appl. Geochem. 25, 288–301. http://dx.doi.org/10.1016/j.apgeochem.2009.11.014.
592

593 Carro B., Borrego J., Morales J.A., 2018. Estuaries of the Huelva Coast: Odiel and Tinto
594 Estuaries (SW Spain). In: Morales J. (eds) The Spanish Coastal Systems. Springer, Cham.
595 Springer Nature Switzerland. https://doi.org/10.1007/978-3-319-93169-2_23.
596
597 Chapin, T.P., 2015. High-frequency, long-duration water sampling in acid mine drainage
598 studies: a short review of current methods and recent advances in automated water
599 samplers. Appl. Geochem. 59, 118–124.
600 http://dx.doi.org/10.1016/j.apgeochem.2015.04.004.
601
602 Chester, R., 1990. Marine Geochemistry. The University Press, Cambridge.
603
604 Cindríc, A.M., Cukrov, N., Durrieu, G., Garnier, C., Pizeta, I., Omanovic, D., 2017.
605 Evaluation of discrete and passive sampling (diffusive gradients in thin-films-DGT)
606 approach for the assessment of trace metal dynamics in marine waters - a case study in a
607 small harbor. Croat. Chem. Acta 90, 177-185. https://doi.org/10.5562/cca3163.
608
609 Dantas, D.V., Barletta, M., Ramos, J.A.A., Lima, A.R.A., Costa, M.F., 2013. Seasonal
610 diets shifts and overlap between two sympatric catfishes in an estuarine nursery. Estuar.
611 Coasts 36, 237–256. https://doi.org/10.1007/s12237-012-9563-2.
612
613 Davis, J.C., 2002. Statistics and Data Analysis in Geology. JohnWiley & Sons, USA.
614
615 Davison, W., Zhang, H., 2012. Progress in understanding the use of diffusive gradients
616 in thin-films – back to basics. Environ. Chem. 2012, 9, 1. doi:10.1071/EN11084.
617

618 Dyer, K.R., 1997. Estuaries: a Physical Introduction, second ed. John Wiley and Sons/
619 Wiley & Sons, Chichester. ISBN: 0-471-9741-4. 195 pp.
620
621 Dunn, R.J.K., Teasdale, P.R., Warnken, J., Schleich, R.R., 2003. Evaluation of the
622 diffusive gradient in a thin film technique for monitoring trace metal concentrations in
623 estuarine waters. Environ. Sci. Technol. 37, 2794-2800.
624 https://doi.org/10.1021/es026425y.
625
626 Dunn, R.J.K., Teasdale, P.R., Warnken, J., Jordan, M.A., Arthur, J.M., 2007. Evaluation
627 of the in situ, time-integrated DGT technique by monitoring changes in heavy metal
628 concentrations in estuarine waters. Environ. Pollut. 148, 213–220.
629 https://doi.org/10.1016/j.envpol.2006.10.027.
630
631 Elbaz-Poulichet, F., Morley, N.H., Beckers, J.M., Nomerange, P., 2001. Metal fluxes
632 through the Strait of Gibraltar: the influence of the Tinto and Odiel rivers (SW Spain).
633 Mar. Chem. 73, 193-213. https://doi.org/10.1016/S0304-4203(00)00106-7.
634
635 EU Commission, 2000. Directive 2000/60/EC of the European Parliament and of the
636 Council, of 23 October 2000, establishing a framework for Community action in the field
637 of water policy. Official Journal of the European Economics L 327/1, 22.12.2000:
638 http://ec.europa.eu/environment/water/water-framework/index_en.html. Last accessed
639 28 October 2019.
640
641 Gao, J., Zhou, C., Gaulier, C., Bratkic, A., Galceran, J., Puy, J., Zhang, H., Leermakers,
642 M., Baeyens. W., 2019. Labile trace metal concentration measurements in marine

643 environments: From coastal to open ocean areas. TRAC-Trend Anal Chem 116,92-101.
644 https://doi.org/10.1016/j.trac.2019.04.027.
645
646 Gaonkar, C.V., Matta, V.M., 2019. Impact of mining on metal concentration in waters of
647 the Zuari estuary, India. Environ Monit Assess 191, 368. https://doi.org/10.1007/s10661-
648 019-7506-0.
649
650 Guéguen, C., Clarisse, O., Perroud, A., McDonald, A., 2011. Chemical speciation and
651 partitioning of trace metals (Cd, Co, Cu, Ni, Pb) in the lower Athabasca River and its
652 tributaries (Alberta, Canada). J. Environ. Monit. 13, 2865-2872.
653 https://doi.org/10.1039/C1EM10563A.
654
655 Hamilton, D.P., Douglas, G. B., Adeney, J. A., Radke, L.C., 2006. Seasonal changes in
656 major ions, nutrients and chlorophyll a at two sites in the Swan River estuary, Western
657 Australia. Mar. Freshwater Res. 57, 803–815.
658
659 Hatje, V., Apte, S.C, Hales, L.T, Birch, G.F, 2003. Dissolved trace metal distributions in
660 Port Jackson estuary (Sydney Harbour), Australia. Mar Pollut Bull 46, 719–730.
661 https://doi.org/10.1016/S0025-326X(03)00061-4.
662
663 Hartnett, M., Wilson, J.G., Nash, S., 2011. Irish estuaries: water quality status and
664 monitoring implications under the water framework directive. Mar. Pol. 35, 810–818.
665 http://dx.doi.org/10.1016/j.marpol.2011.01.010.
666

667 Hierro, A., Olías, M., Ketterer, M.E., Vaca, F., Borrego, J., Cánovas, C.R., Bolívar, J.P.,
668 2014a. Geochemical behavior of metals and metalloids in an estuary affected by acid
669 mine drainage (AMD). Environ. Sci. Pollut. Res. 21, 2611-2627. DOI 10.1007/s11356-
670 013-2189-5.
671
672 Hierro, A., Olías, M., Cánovas, C.R., Martín, J.E., Bolivar, J.P., 2014b. Trace metal
673 partitioning over a tidal cycle in an estuary affected by acid mine drainage (Tinto estuary,
674 SW Spain). Sci. Total Environ. 497-498, 18-28.
675 https://doi.org/10.1016/j.scitotenv.2014.07.070.
676
677 Johnson, J., Oelkers, E., Helgeson, H., 1992. SUPCRT92: a software package for
678 calculating the standard molal thermodynamic properties of minerals, gases, aqueous
679 species and reactions from 1 to 5000 bar and 0 to 1000 °C. Comput. Geosci. 18, 899–947.
680
681 Liu, R., Lead, J.R., Zhang H., 2013. Combining cross flow ultrafiltration and diffusion
682 gradients in thin-films approaches to determine trace metal speciation in freshwaters.
683 Geochim. Cosmochim. Acta 109, 14–26. http://dx.doi.org/10.1016/j.gca.2013.01.030.
684
685 Lucas, A.R., Salmon, S.U, Rate, A.W., Larsen, S., Kilminster, K., 2015. Spatial and
686 temporal distribution of Au and other trace elements in an estuary using the diffusive
687 gradients in thin films technique and grab sampling. Geochim. Cosmochim. Acta 171,
688 156-173. http://dx.doi.org/10.1016/j.gca.2015.08.025.
689
690 Machado, A.A.d.S., Spencer, K., Kloas, W., Toffolon, M., Zarfl, C., 2016. Metal fate and

691 effects in estuaries: a review and conceptual model for better understanding of toxicity.
692 Sci. Total Environ. 541,268–281. http://dx.doi.org/10.1016/j.scitotenv.2015.09.045.
693
694 Mangal, V., Zhu, Y., Shi, Y.X., Guéguen, C., 2016. Assessing cadmium and vanadium
695 accumulation using diffusive gradient in thin-films(DGT) and phytoplankton in the
696 Churchill River estuary, Manitoba. Chemosphere 163, 90-98.
697
698 Millero, F.J., Woosley, R., Ditrolio, B., Waters, J., 2009. Effect of Ocean acidification on
699 the speciation of metals in seawater. Oceanography 22 (4).
700 https://doi.org/10.5670/oceanog.2009.98.
701
702 Montero, N., Belzunce-Segarra, M.J., Gonzalez, J.L., Larreta, J., Franco, J., 2012.
703 Evaluation of diffusive gradients in thin-films (DGTs) as a monitoring tool for the
704 assessment of the chemical status of transitional waters within the Water Framework
705 Directive. Mar. Pollut. Bull. 64 (1), 31-39.
706 https://doi.org/10.1016/j.marpolbul.2011.10.028.
707
708 Montero, N., Belzunce-Segarra, M.J., Del Campo, A., Garmendia, J.M., Ferrer, L.,
709 Larreta, J., González, M., Maidana, M.A., Espino, M., 2013. Integrative environmental
710 assessment of the impact of Pasaia harbor activities on the Oiartzun estuary (southeastern
711 Bay of Biscay). J. Mar. Syst. 109-110, S252–S260. doi: 10.1016/j.jmarsys.2011.06.002.
712
713 Morillo, J., Usero, J., 2008. Trace metal bioavailability in the waters of two different
714 habitats in Spain: Huelva estuary and Algeciras Bay. Ecotox. Environ. Safe 71, 851–859.
715 doi:10.1016/j.ecoenv.2008.01.016.

716

717 Nieto, J.M, Sarmiento, A.M, Olías, M., Cánovas, C.R, Riba, I., Kalman, J., Delvalls T.A,
718 2007. Acid mine drainage pollution in the Tinto and Odiel Rivers (Iberian Pyrite Belt,
719 SW Spain) and bioavailability of the transported metals to the Huelva estuary. Environ.
720 Int. 33, 445–455. doi:10.1016/j.envint.2006.11.010.

721

722 NIST, 2004. In: Martell, A.E., Smith, R.M. (Eds.), NIST Standard Reference Database
723 46 Version 8.0, Gaithersburg, USA.

724

725 Nordstrom, D.K., Wilde, F.D., 1998. Reduction-oxidation potential (electrode method).
726 National Field Manual for the Collection of Water Quality Data. U.S. Geological Survey
727 Techniques of Water-Resources Investigations, U.S. Geological Survey, Reston, VA, p.
728 20. Book 9, (Chapter 6).5.

729

730 Olías, M., Cánovas, C.R., Basallote, M.D., Macías, F., Pérez-López, R., Moreno
731 González, R., Millán-Becerro, R., Nieto, J.M., 2019. Causes and impacts of a mine water
732 spill from an acidic pit lake (Iberian Pyrite Belt). Environ. Pollut. 250, 127-136.
733 https://doi.org/10.1016/j.envpol.2019.04.011.

734

735 Panther, J.G., Bennett, W.W., Welsh, D.T., Teasdale, P.R., 2014. Simultaneous
736 measurement of trace metal and oxyanion concentrations in water using diffusive
737 gradients in thin films with a chelex-metsorb mixed binding layer. Anal. Chem. 86, 427-
738 434. https://doi.org/10.1021/ac402247j.

739

740 Parkhurst, D.L., Appelo, C.A.J., 2013. Description of input and examples for PHREEQC
741 version 3.4—a computer program for speciation, batch-reaction, one-dimensional
742 transport, and inverse geochemical calculations. In: U.S. Geological Survey Techniques
743 and Methods, book 6, chap. A43, pp. 497.
744
745 Pérez-López, R., Macías, F., Cánovas, C.R., Sarmiento, A.M., Pérez-Moreno, S.M.,
746 2016. Pollutant flows from a phosphogypsum disposal area to an estuarine environment:
747 an insight from geochemical signatures. Sci. Total Environ. 553, 42–51.
748 https://doi.org/10.1016/j.scitotenv.2016.02.070.
749
750 Schintu, M., Durante, L., Maccioni, A., Meloni, P., Degetto, S., Contu, A., 2008.
751 Measurement of environmental trace-metal levels in Mediterranean coastal areas with
752 transplanted mussels and DGT techniques. Mar. Pollut. Bull. 57, 832-837.
753 https://doi.org/10.1016/j.marpolbul.2008.02.038.
754
755 Sherwood, J.E., Barnett, D., Barnett, N.W., Dover, K., Howitt, J., Li, H., Kew, P.,
756 Mondon, J., 2009. Deployment of DGT units in marine waters to assess the environmental
757 risk from a deep sea tailings outfall. Anal. Chim. Acta 652, 215–223.
758
759 Shiva, A.H., Bennett, W.W., Welsh, D.T., Teasdale, P.R., 2016. In situ evaluation of DGT
760 techniques for measurement of trace metals in estuarine waters: a comparison of four
761 binding layers with open and restricted diffusive layers, Environ. Sci. Process. Impacts
762 18, 51-63. https://doi.org/10.1039/C5EM00550G.
763

764 Spencer, K.L., MacLeod, C.L., Tuckett, A., Johnson, S.M., 2006. Source and distribution
765 of trace metals in the Medway and Swale estuaries, Kent. Mar. Pollut. Bull. 52, 226–231.
766 DOI: 10.1016/j.marpolbul.2005.10.019.
767
768 Thanh-Nho, N., Strady, E., Nhu-Trang, T.T., David, F., Marchand, C., 2018. Trace metals
769 partitioning between particulate and dissolved phases along a tropical mangrove estuary
770 (Can Gio, Vietnam). Chemosphere 196, 311-322.
771 https://doi.org/10.1016/j.chemosphere.2017.12.189.
772
773 Turner, A., 2014. Mobilisation and bioaccessibility of lead in paint from abandoned boats.
774 Mar. Pollut. Bull. 89, 35–39. doi:10.1016/j.marpolbul.2014.10.038.
775
776 Tusseau-Vuillemin, M.H., Gilbin, R., Bakkaus, E., Garric, J., 2004. Performance of
777 diffusion gradient in thin films to evaluate the toxic fraction of copper to Daphnia magna.
778 Environ. Toxicol. Chem. 23 (9), 2154-2161. DOI: 10.1897/03-202a.
779
780 Unsworth E. R., Warnken K. W., Zhang H., Davison W., Black F., Buffle J., Cao J.,
781 Cleven R., Galceran J., Gunkel P., Kalis E., Kistler D., van Leeuwen H. P., Martin M.,
782 Noel S., Nur Y., Odzak N., Puy J., van Riemsdijk W., Sigg L., Temminghoff E., Tercier-
783 Waeber M.-L., Toepperwien S., Town R. M., Weng L., Xue H. (2006) Model predictions
784 of metal speciation in freshwaters compared to measurements by in situ techniques.
785 Environ. Sci. Technol. 40, 1942–1949. https://doi.org/10.1021/es051246c.
786
787 Van Geen, A., Boyle, E.A., Moore, W., 1991. Trace metal enrichments in waters of the
788 Gulf of Cadiz, Spain. Geochim. Cosmochim. Acta 55, 2173-2191.

Verweij, W., 2017. Manual for CHEAQS Next, a Program for Calculating Chemical Equilibria in Aquatic Systems.

Vicente-Martorell, J.J., Galindo-Riaño, M.D., García-Vargas, M., Granado-Castro, M.D., 2009. Bioavailability of heavy metals monitoring water, sediments and fish species from a polluted estuary. J. Hazard. Mater. 162 (2), 823–836. https://doi.org/10.1016/j.jhazmat.2008.05.106.

Ytreberg, E., Bighiu, M.A., Lundgren, L., Eklund, B., 2016. XRF measurements of tin, copper and zinc in antifouling paints coated on leisure boats. Environ. Pollut. 213, 594-599. https://doi.org/10.1016/j.envpol.2016.03.029.

Tables

Sample	Tide Conditions	Temperature (ºC)	pH	ORP (mV)	Chlorinity (g/L)	Salinity (g/L)
T1	Low tide	24.0	8.1	206	18	33
T1	High tide	26.9	8.1	195	19	34
T1	Low tide	24.0	7.7	206	18	33
T1	High tide	26.9	8.0	195	19	34
T2	Low tide	24.9	7.9	213	18	33
T2	High tide	25.4	8.3	202	19	34
T2	Low tide	24.9	8.1	213	18	33
T2	High tide	25.4	8.3	202	19	34
T3	Low tide	24.5	8.4	171	18	33
T3	High tide	25.5	8.3	187	19	34
T3	Low tide	24.5	8.1	171	19	34
T3	High tide	25.5	8.2	187	19	34
T4	Low tide	20.7	8.2	400	19	34
T4	High tide	21.9	8.4	202	20	37
T4	Low tide	20.7	8.2	193	19	34
T4	High tide	21.9	8.4	202	20	37
Minimum		20.7	7.7	171	18	33
Maximum		26.9	8.4	400	20	37
Mean		24.2	8.2	209	19	34
S.D		2.0	0.2	52	0.7	1.2

Table 1. Main physico-chemical properties of samples collected in the Ria of Huelva estuary (SW Spain). S.D: standard deviation

Table 1. Table 1. Main physico-chemical properties of samples collected in the Ria of Huelva estuary (SW Spain). S.D: standard deviation.

Estuary	Salinity	As	Cd	Co	Cu	Fe	Mn	Ni	Pb	Sb	Sn	V	Zn
Ria of Huelva (Spain, this study)	33-37	8.7	1.4	1.7	21	14	65	1.7	2.7	0.92	0.05	1.3	50
Port Jackson (Australia)[1]	21-35		0.04		1.7		20	0.86					6.5
Goa (India)[2]	0.7-29				2.1-2.2	40-45	2.7-3.72		5.7-7.2				22-36
Can Gio (Vietnam)[3]	7.4-23	0.15	0.45	0.05	0.30-1.8	1.0-5.0	0.98-1.15	0.30-1.8	0.03-0.30				
San Francisco (USA)[4]	>20	2.1	0.06	0.2	1.8	32	44	2.2	0.064				1.6

1. Hatje et al. 2003
2. Gaonkar and Matta 2019
3. Thanh-Nho et al. 2018
4. Benoit et al. 2010

821

822 **Table 2.** Salinity (g L^{-1}) and average dissolved metal content (in µg L^{-1}) in the Ria de
823 Huelva estuary (SW Spain) and comparison with others estuaries affected by
824 anthropogenic activities worldwide.

Estuary	As	Cd	Co	Cu	Fe	Mn	Ni	Pb	Sb	Sn	V	Zn
Ria of Huelva (Spain, this study)	0.12-1.3	0.10-2.3	0.07-8.7	4.6-23	8.1-45	4.8-61	n.d	0.30-8.0	0.02-0.21	0.04-0.41	0.85-1.3	33-165
Bay of Biscay estuaries, Spain[1]		0.24-1.57		0.21-0.26			0.16-0.17					2.8-3.4
Runaway Bay Marina, Australia[2]	0.81	0.04	0.09	2.7		8.6	0.32	0.02	0.10		1.5	3.4
Brown and O'Brien Bay, Antarctica, Australia[3]	0.001-0.003	0.07-0.09	0.005-0.03	1.0-2.0	0.2-0.5	0.1-0.9	0.3-0.4	0.3-0.6		0.003-0.004		3.0-10
Patos Lagoon, Brazil[4]		0.01-0.03	0.006-0.01	0.1-0.4		5.0-6.0	0.1-0.3					0.5-2.1
Jiulong estuary, China[5]		0.04-0.12	0.15-0.95	2.8-13			4.6-26	0.05-0.39				79-195
Gold Coast (Australia)[6]		0.009-0.024	0.074-0.101	0.8-2.3	6.3-10	6.7-22	0.3-0.5	.017-0.037				10.9-27

1. Montero et al., (2012)
2. Shiva et al. (2016)
3. Larner et al. (2006)
4. Wallner-Kersanach et al. (2006)
5. Weng and Wang (2014)
6. Waltham et al., (2011)

825

826 **Table 3.** Concentrations in DGTs (in µg L-1) deployed along the Ria de Huelva estuary
827 and comparison with values reported in other estuaries worldwide

828

829

830

831

832

833

834

835

Figures

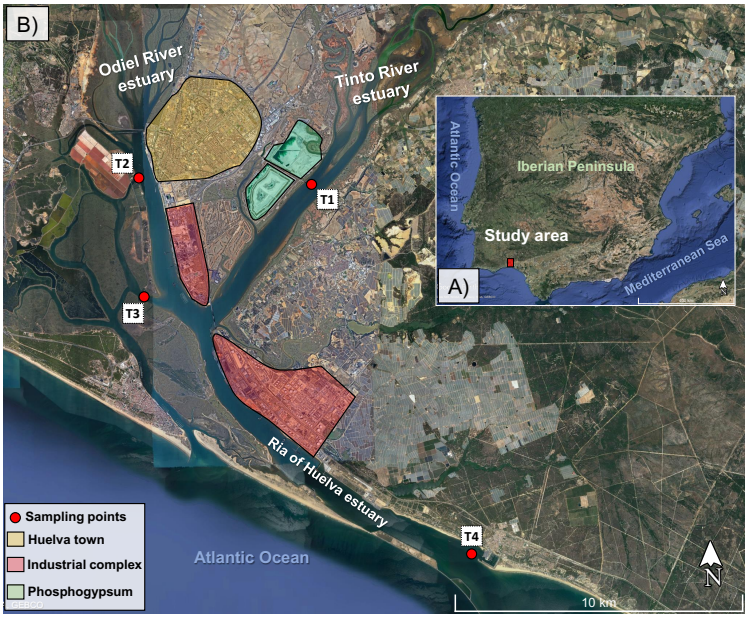

Figure 1. Location map of the study area (A), showing the sampling stations (T1-T4) and main anthropogenic activities (B): the city of Huelva (marked off yellow shadow); the Industrial complex (red shadow area) and the phosphogypsum stacks (green shadow) .

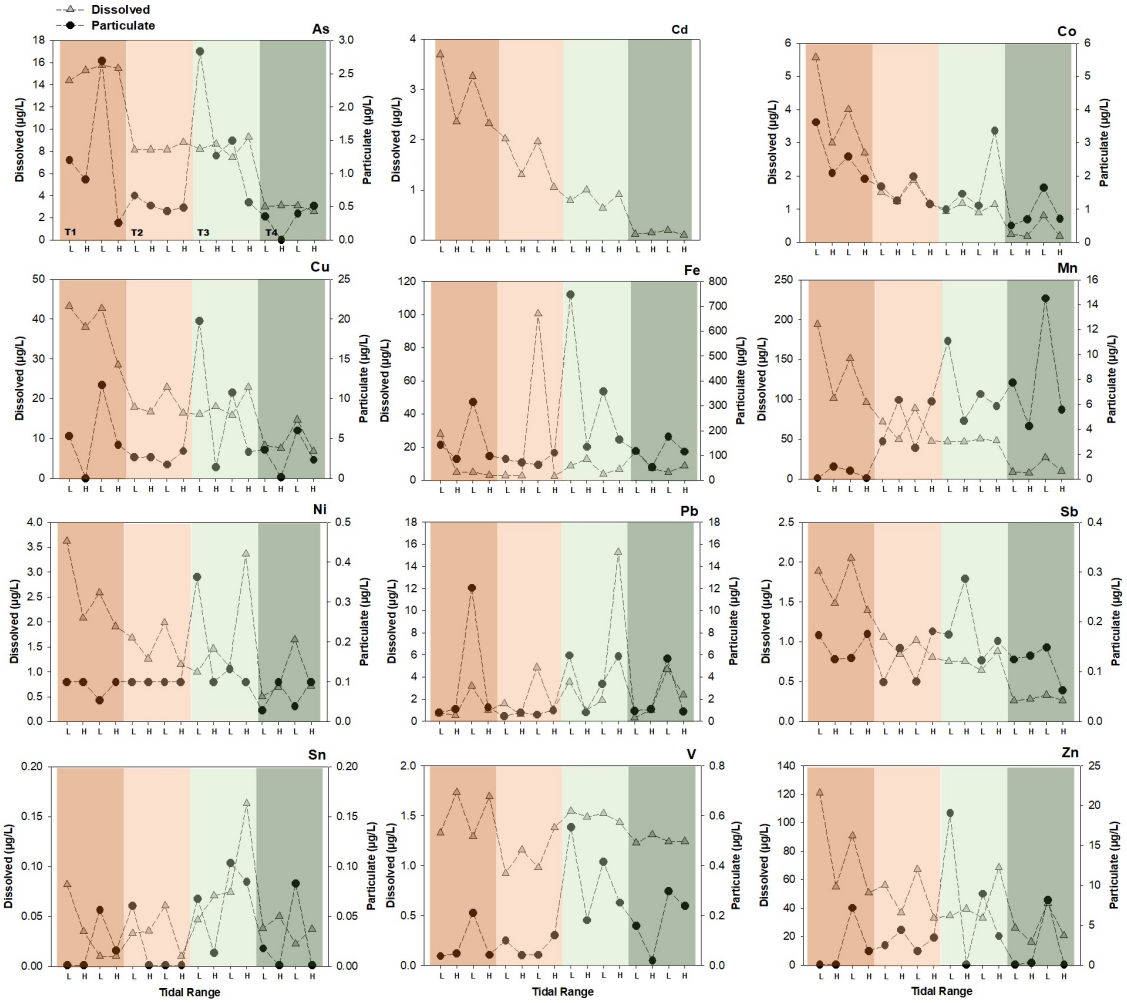

841

842 **Figure 2.** Evolution of dissolved (triangle dashed line) and particulate (dark-circle dashed
843 line) concentrations of metals in the estuary for the 4 sampling sites (T1; dark-orange
844 shadow, T2; light-orange shadow, T3; whitish shadow and T4; greenish shadow) and for
845 the 4 sampling times (L: low tide; H: high tide). Cd particulate concentrations were below
846 detection limit of the equipment.

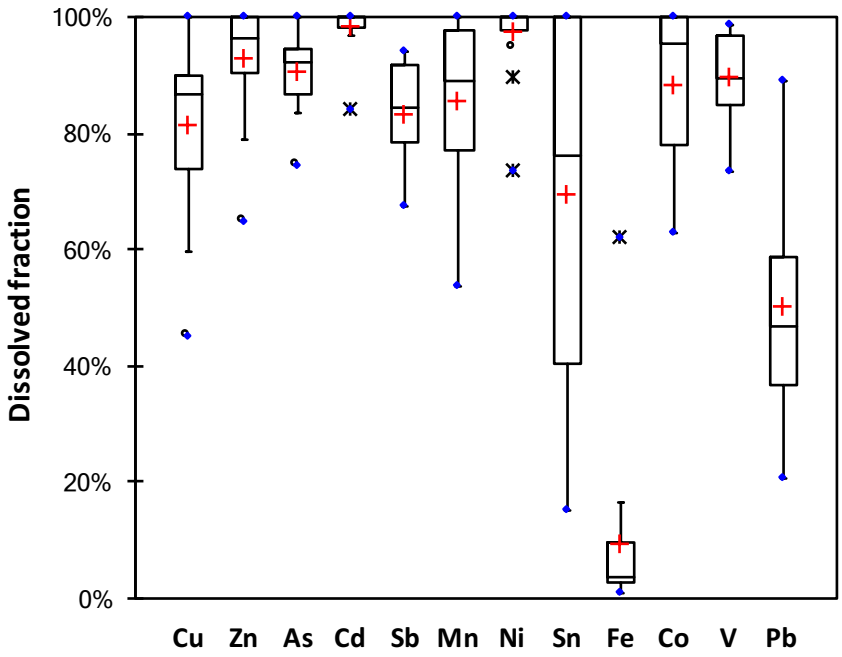

847

848 **Figure 3.** Box and whiskers plot of the percentage of elements in the dissolved fraction

849 (see text for explanation).

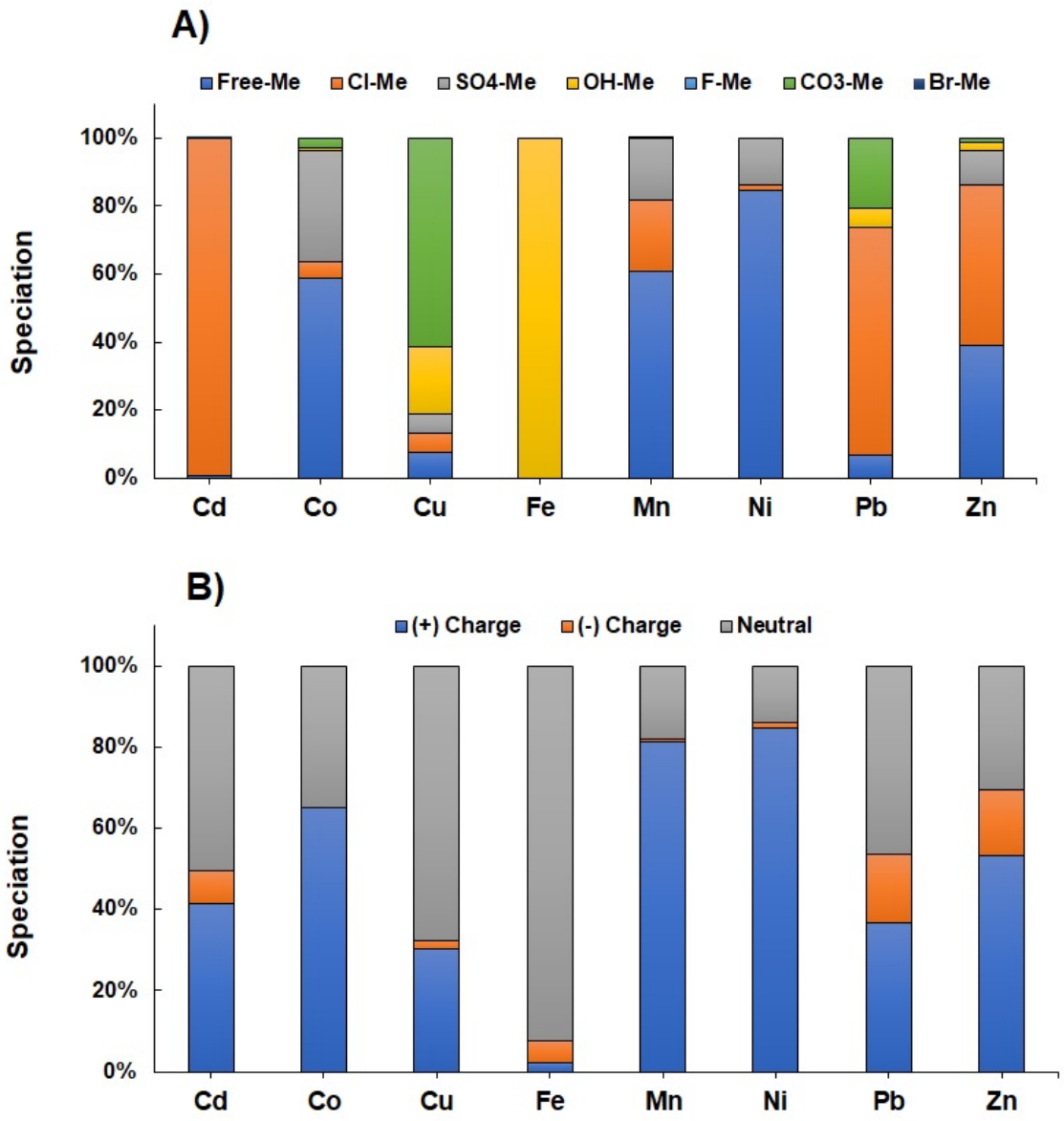

850

851 **Figure 4.** Metal/loid speciation of estuarine waters considering complex type (A); Free
852 metal (Free-Me), Chloride complex metal (Cl-Me), Sulfate complex Metal (SO_4-Me),
853 Hydroxyl complex metal (OH-Me), Fluoride complex metal (F-Me), Carbonate complex
854 metal (CO_3-Me), Boride complex metal (B-M), Oxide complex metal (O-Me); and charge
855 (B).

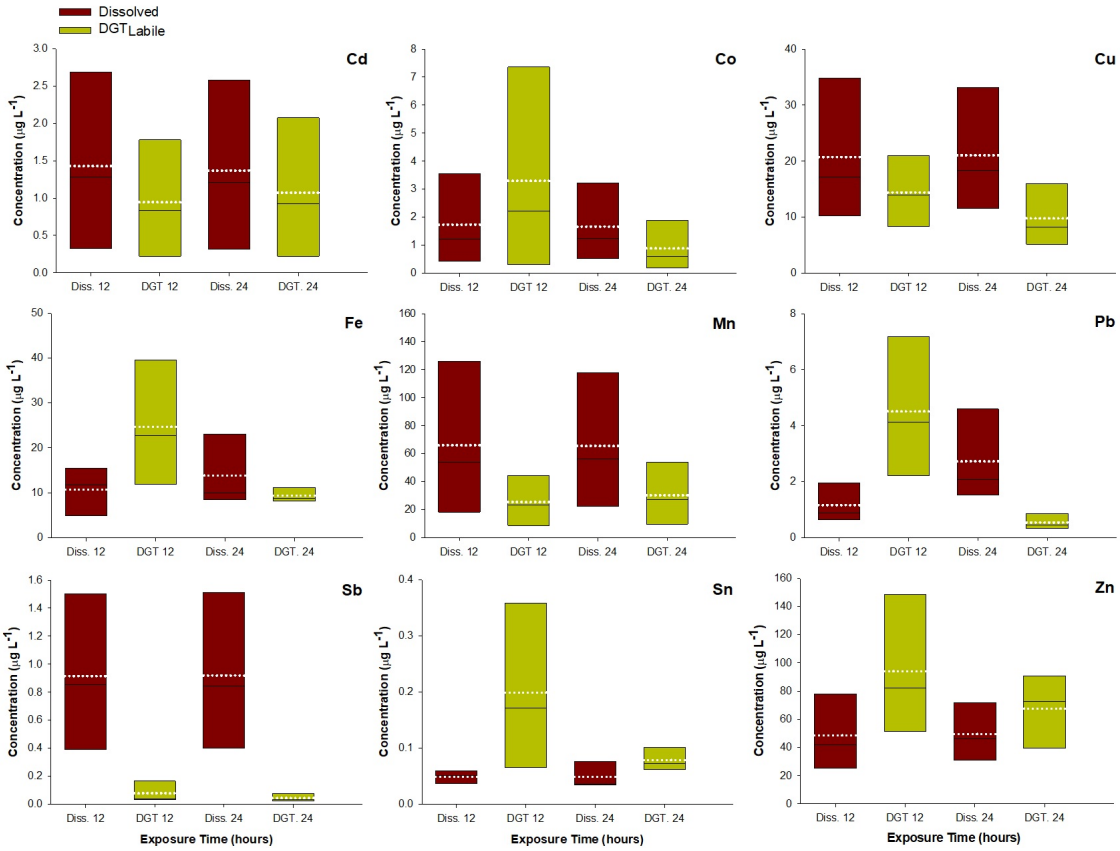

856

857 **Figure 5.** Average dissolved metal concentration (red bars) and DGT concentration (light
858 green bars) in the water column, for all the sampling stations, for the two DGT exposure
859 periods (12 and 24 h). Dissolved concentrations result from the average concentration for
860 the first two low and high tides (Diss. 12) and for the two complete tidal cycles measured
861 (Diss 24). Horizontal black and white dotted lines represent the median and mean values,
862 respectively.

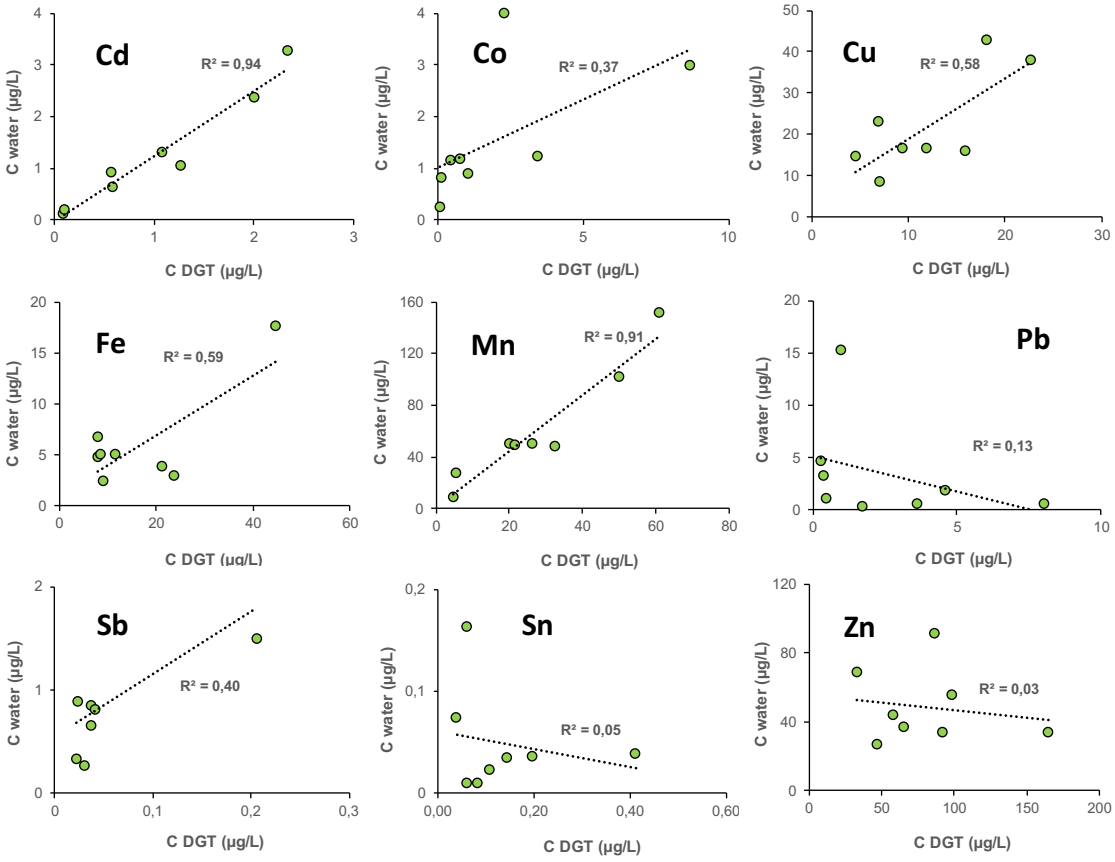

863

864 **Figure 6.** Relationship between the metal/loid concentration in DGT (C_{DGT}) and the

865 dissolved concentration (C_{Water}).

866

867

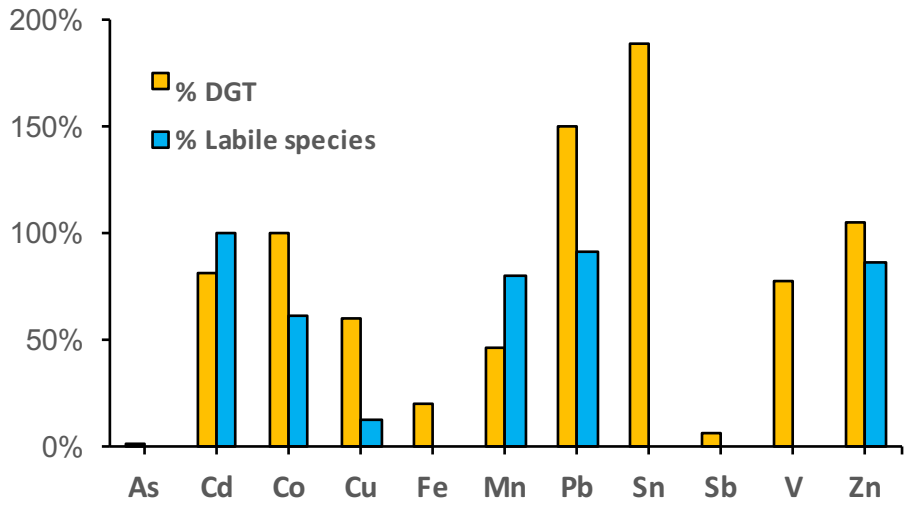

868

869 **Figure 7.** Comparison between the average content of labile species (in blue) of
870 metal/loid and the percentage of DGTs (C_{DGT}) concentration with respect the
871 concentration of the water column (in orange). C_{DGT} for Fe, Sn, Pb and Zn are compared
872 with total concentration (see text for explanation).

873

874